Physics of the Solid State, 2023, Vol. 65, No. 12

03,05

# Ferromagnetic GaMnAs layers obtained by implantation of manganese ions followed by pulsed laser annealing

© Yu.A. Danilov[1], Yu.A. Agafonov[2], V.I. Bachurin[3], V.A. Bykov[1], O.V. Vikhrova[1], V.I. Zinenko[2], I.L. Kalentyeva[1], A.V. Kudrin[1], A.V. Nezhdanov[1], A.E. Parafin[4], S.G. Simakin[3], P.A. Yunin[4], A.A. Yakovleva[1]

[1] Lobachevsky State University,
Nizhny Novgorod, Russia
[2] Institute of Microelectronics Technology and High Purity Materials, Russian Academy of Sciences,
Chernogolovka, Russia
[3] Valiev Institute of Physics and Technology of RAS, Yaroslavl Branch,
Yaroslavl, Russia
[4] Institute for Physics of Microstructures, Russian Academy of Sciences,
Nizhny Novgorod, Russia

E-mail: danilov@nifti.unn.ru

Received October 17, 2023
Revised October 17, 2023
Accepted October 24, 2023

Using the methods of secondary ion mass spectrometry, X-ray diffraction, Raman scattering, measurements of the Hall effect and magnetoresistance, and magnetic circular dichroism, an experimental study of the properties of layers obtained by implanting manganese ions (energy of 180 keV) into semi-insulating gallium arsenide was carried out, followed by annealing with a KrF excimer laser pulse. It has been shown that at ion doses from $1 \cdot 10^{16}$ to $5 \cdot 10^{16}\,\mathrm{cm}^{-2}$ and a laser energy density of $300\,\mathrm{mJ/cm}^2$, heavily doped layers of $p$-type conductivity are formed, which, according to the results of studies by different methods, have ferromagnetic properties with a Curie temperature that depends on the dose ions and reaching 120 K. The influence of ion sputtering on impurity profiles is considered and taken into account in this work. It was found that during subsequent laser annealing, segregation of Mn atoms to the GaAs surface is observed.

**Keywords:** gallium arsenide, implantation of Mn ions, laser annealing, anomalous Hall effect, ferromagnetism, Curie temperature.

DOI: 10.61011/PSS.2023.12.57686.230

## 1. Introduction

Diluted magnetic semiconductors (DMS), which, in addition to semiconductor properties, also have ferromagnetic properties, are one of the main materials of spin electronics, performing the functions, for example, of a spin injector. Their production requires introducing into the semiconductor of the impurities of transition elements in concentrations of at least several at.% [1]. The canonical DMS, on which many design options for spin electronics devices are being developed [2], — GaMnAs, which usually has a Curie temperature of about 100−110 K. A feature of manganese behavior in GaAs is that Mn atoms occupy predominantly Ga positions, where, in addition to introducing into the crystal lattice of uncompensated magnetic moments due to the unfilled $3d$-shell, they are acceptors with an ionization energy of 0.113 eV (at relatively low impurity concentrations) above the valence band top [3]. The latter circumstance leads to the fact that GaAs heavily-doped with manganese also has a high concentration of free charge carriers, and this provides indirect mechanism of the ferromagnetic ordering of the magnetic moments of Mn atoms.

To obtain GaMnAs in laboratory conditions, low-temperature molecular beam epitaxy (LT-MBE) is usually used, but the high cost of equipment and low productivity do not allow this method use for any large-scale production. A solution may be to introduce manganese through the use of ion implantation (II) — the only semiconductor doping method used in modern technology of integrated circuit manufacturing. However, a large concentration of radiation defects created during the GaAs irradiation with Mn ions (and, as a rule, amorphization) requires post-implantation annealing to eliminate violations of the crystal structure and to activate impurities.

At the first stages of testing the technology of GaAs ion doping with manganese, thermal annealing was used for post-implantation treatment with a process duration of about tens of seconds (rapid thermal annealing) [4–6]. It turned out, however, that the annealed layers contain clusters of the ferromagnetic phase formed during thermal heating due to the reaction of excess Mn atoms (above the limit of equilibrium solid solubility, estimated as $\sim 3 \cdot 10^{19}\,\mathrm{cm}^{-2}$ [7]) with components of base semiconductor. In this case, the formation of two systems of clusters was observed: clusters of MnAs composition buried at a depth about the

average projected range of Mn ions in GaAs, and surface clusters of GaMn [5]. Therefore, the rapid thermal annealing procedure is not suitable for the formation of a single-phase semiconductor layer GaMnAs.

Further studies showed [8] that the use of the method (by this time supposedly forgotten) of nanosecond pulsed laser annealing (PLA) for treatment of GaAs irradiated with large doses of Mn ions allows the effects minimization of cluster formation due to a significant reduction in time of plate heating and speed increasing of the recrystallization front movement from the single-crystal substrate to the surface. Studies, mainly by two groups (Dubon et al. [8] and S. Zhou et al. [9]), showed the fundamental possibility of forming a single-phase ferromagnetic semiconductor GaMnAs by implanting large doses (up to $5 \cdot 10^{16}\,\mathrm{cm}^{-2}$) of $Mn^+$ ions into semi-insulating GaAs with subsequent annealing a single pulse, usually from an excimer laser.

Our paper [10] confirmed the formation of GaMnAs DMS as a result of II + PLA process implementation. However, note that the process of ion implantation includes a complex set of phenomena, especially when introducing heavy ions with high doses. Among these phenomena, which are not sufficiently covered in papers on the GaMnAs production, one can note ion sputtering (depending in turn on the energy of the ions), uncontrolled heating of plates irradiated by ions in the process of dose accumulation, the influence of the surface condition on the migration of radiation defects during storage and annealing of samples irradiated by ions. Therefore, the comparison of the results of ion-implantation formation of GaMnAs under different experimental conditions is of significant interest both from a methodological point of view and in terms of the practical implementation of the method.

The purpose of this paper is to study the influence of the conditions of GaAs irradiation with Mn ions (primarily dose) on the electrical, optical and magnetic properties of layers formed in the procedure of „ion implantation plus pulsed laser annealing".

## 2. Experimental procedure

Epi-ready semi-insulating GaAs plates with crystal-lattice orientation of surface (100) were used as the initial material. Implantation of ions $Mn^+$ with an energy of 180 keV was performed on accelerator Extrion 200-1000 (Varian). Radiation doses were $1 \cdot 10^{16}$, $3 \cdot 10^{16}$ and $5 \cdot 10^{16}\,\mathrm{cm}^{-2}$.

It makes sense to explain the choice of energy for implantation of manganese ions into GaAs. On the one hand, the thickness of the layer, in which the main part of the implanted ions is located, increases with increase in irradiation energy ($E$). Thus, the thickness of the implanted GaAs:Mn layer calculated using the SRIM-2013.00 program [11] varies from $\sim 70$ nm for $E = 50$ keV to $\sim 300$ nm for $E = 240$ keV. On the other hand, the ion sputtering coefficient depends on the implantation energy. Sputtering ratio ($S$), also calculated by the SRIM-2013.00 code, increases from 6.49 (for $E = 240$ keV) to value of 9.63 for $E = 30$ keV. Consequently, at relatively low implantation energies and high doses a significant portion of the doped layer is etched away during the irradiation process, and high dopant concentrations achievement can become a challenge. The thickness of the etched down layer can be estimated by the formula $d_s = (SD)/N$, where $N$ — number of target atoms per unit volume, $D$ — ion dose. For example, at the implantation dose of $3 \cdot 10^{16}\,\mathrm{cm}^{-2}$ and energy of 50 keV the value $d_s = 64$ nm (the sum of the calculated average projected range $R_p$ and straggling ranges $\Delta R_p$is equal to 49.8 nm). For 180 keV and the same dose, the calculated thickness of the etched down layer is 48 nm, which is $\sim 31\%$ of the value $R_p + \Delta R_p = 154.3$ nm (the latter value can serve as rough estimate of the total range of ions Mn). Based on these considerations and the capabilities of the available accelerating technology, the implantation energy was chosen to be 180 keV.

Post-implantation annealing of the samples was carried out with a pulse from LPX-200 excimer laser with a working mixture of KrF. A radiation beam was used, the cross section of which at the sample location was about $1 \times 1.5$ cm. Laser pulse parameters: radiation wavelength 248 nm, pulse duration 30 ns, energy density $300\,\mathrm{mJ/cm^2}$ (this energy density value is close to the optimal annealing conditions used in a number of papers and, in particular, [9]).

The composition and distribution profiles of Mn atoms over the depth of the doped layer were studied by secondary ion mass spectrometry (SIMS) using IONTOF5 setup with a time-of-flight mass analyzer. Probing was carried out with a beam of bismuth ions (25 keV), and sputtering was performed during layer-by-layer analysis using oxygen ions with an energy of 1 keV. The sputtering time scale was converted into a depth scale using measurements of the final depth of the formed crater on a Talystep profilometer with an error of no more than 2%. Calibration for the concentration of Mn atoms was performed by normalizing the integral under the experimental profile to the implantation dose (taking into account the calculated losses due to sputtering).

The structure of the implanted layers was studied by high-resolution X-ray diffractometry (HRXRD) on a Bruker D8 Discover diffractometer.

Raman scattering (RS) spectra were studied at 300 K using NTEGRA Spectra complex. A laser with a wavelength of 473 nm was used; its radiation was focused by a lens 100× with an aperture NA = 0.9. Laser radiation power measured using 11PD100-Si (Standa Ltd) silicon photodetector was equal to 0.5 mW. RS spectra were analyzed within range $50-900\,\mathrm{cm}^{-1}$ with resolution $0.7\,\mathrm{cm}^{-1}$. The exposure time was 120 s. Backscatter geometry was used.

Galvanomagnetic properties were studied by scanning magnetic field applied perpendicular to the surface of the structures in the range $\pm 3600$ Oe. In this case, the samples were placed in Janis CCS-300S/202 closed-cycle

helium cryostat, and measurements were performed using a Keithley 2400 source meter at temperatures 10–300 K.

Magnetic circular dichroism (MCD) studies were carried out in the spectral range 1.15–2.5 eV for the geometry of reflection of circularly polarized light from the surface of structures. The external magnetic field was applied perpendicularly to the plane of the sample. The magnitude of the MCD effect was determined as the ratio of the difference in intensities of light reflected from the sample with left and right circular polarization to the total light intensity.

## 3. Experimental results

Figure 1 shows the distribution profiles of Mn atoms in GaAs after implantation with dose $3 \cdot 10^{16}\,\text{cm}^{-2}$. There is good agreement between the experimental profile (2), obtained by the SIMS method, and the profile (1), calculated using SRIM-2013.00 code and corrected for sputtering (calculated ion sputtering coefficient $S = 7.13$ for energy of 180 keV). As a result of pulsed laser annealing, significant changes in the profile occurred: (3) strong segregation of Mn atoms to the surface is observed, and inside the layer 60–170 nm — a non-bell-shaped distribution with an average value $N_{\text{av}}$ about $1 \cdot 10^{21}\,\text{cm}^{-3}$. The initial impurity distribution and the Mn profile after annealing coincide well only in limited regions 35–60 and 180–220 nm, where the concentrations of implanted Mn are relatively low. Similar profiles (Mn segregation to the surface and a decrease of concentration in the layer compared to the initial distribution) are also observed for doses $1 \cdot 10^{16}\,\text{cm}^{-2}$ ($N_{\text{av}} \approx 3.5 \cdot 10^{20}\,\text{cm}^{-3}$) and $5 \cdot 10^{16}\,\text{cm}^{-2}$ ($N_{\text{av}} \approx 2 \cdot 10^{21}\,\text{cm}^{-3}$).

Analysis of X-ray diffraction spectra — HRXRD (Figure 2) shows the presence of an inhomogeneously deformed GaMnAs layer, as can be seen from the asymmetric peak on 65.75° on $2\theta$ to the left of the peak of the GaAs substrate (on 66.05°) with thickness contrast oscillations located only on one side of the layer peak. The deformation profile obtained by fitting the HRXRD curve in the Bruker Diffrac.Leptos software package for an implanted but unannealed sample is shown in Figure 1 (curve *4*). The profile qualitatively corresponds to the calculated and measured Mn distribution in the implanted sample. The kink in the profile is a consequence of the model limitations for specifying deformation gradients used by the program. As a result of PLA, noticeable changes in the HRXRD spectrum occurred (Figure 2): oscillations to the left of the GaAs (004) peak disappeared, the peak of the deformed material shifted slightly to the angle $2\theta = 65.8°$ closer to the substrate peak. A weak, broad peak appeared to the right of the substrate peak. Qualitatively similar patterns were observed for other doses of Mn ions implantation.

A decrease in the peak shift after annealing indicates decrease in deformation as a result of both defects annealing

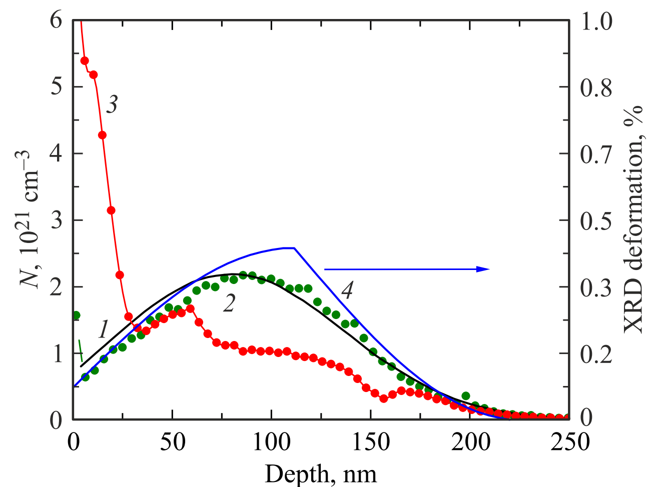


**Figure 1.** Depth distribution profiles of Mn atoms (implantation with a dose $3 \cdot 10^{16}\,\text{cm}^{-2}$ at energy of 180 keV) in GaAs: *1* — modeling with the SRIM code taking into account sputtering; *2* — SIMS data after implantation; *3* — SIMS data after annealing; *4* — GaAs deformation profile for implanted unannealed sample according to HRXRD data.

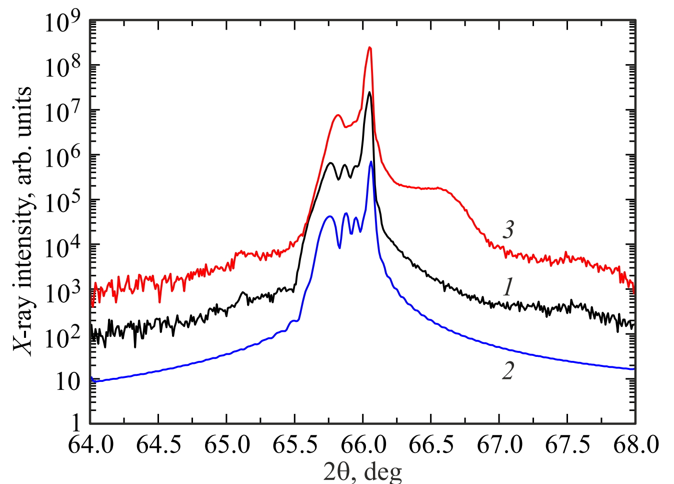


**Figure 2.** Diffraction patterns of GaAs plate irradiated with Mn ions (dose $3 \cdot 10^{16}\,\text{cm}^{-2}$ at energy of 180 keV) before (curve *1*) and after annealing (curve *3*). The curve of the ion-implanted unannealed sample was approximated (the fit is shown by curve *2*) using a gradient deformation model, see curve *4* in Figure 1.

in the GaMnAs layer, and a decrease in Mn concentration in the layer due to segregation. The appearance of a weak and broad peak to the right of the substrate peak in some publications [12] is associated with the formation of MnAs clusters, which, however, is not directly confirmed. Comparing the HRXRD data with SIMS, it can be assumed that the appearance of the weak and broad peak to the right of the substrate peak is associated with thin near-surface layer (thickness about 10 nm) of GaAs with a high concentration of „non-structural“ manganese. The formation of islands of the GaAs defect

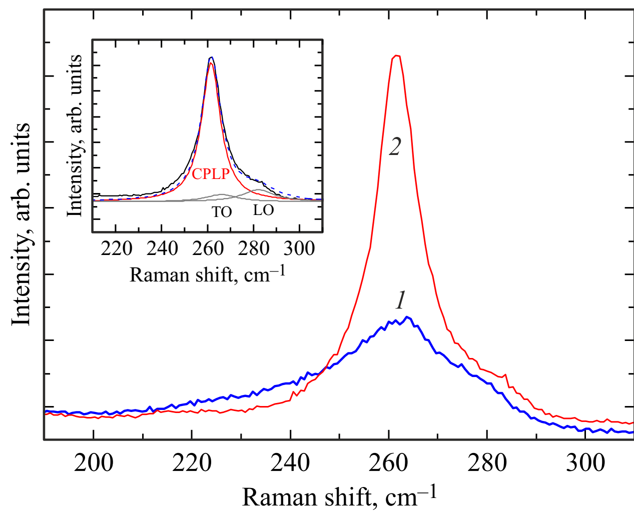


**Figure 3.** Raman scattering spectra GaAs samples irradiated with Mn ions with dose $5 \cdot 10^{16}$ cm$^{-2}$ before (*1*) and after (*2*) pulsed laser annealing. The insert shows decomposition of the spectrum *2* into Lorentzians.

phase stretched in the plane in this layer cannot be excluded. At the same time, the main volume of the implanted layer, according to both SIMS and HRXRD, is an DMS GaMnAs.

Figure 3 shows the Raman scattering spectra of samples irradiated with Mn ions before and after laser annealing.

In the spectrum of the unannealed sample irradiated with ions, a rather wide asymmetric band is observed near the wave number 263 cm$^{-1}$. After laser annealing the spectrum changes significantly: an asymmetric peak appears, which can be represented by the sum of three Lorentzians: two low-intensity bands with maximum positions of 282 and 266 cm$^{-1}$, and one intense peak with a maximum position of about 261.5 cm$^{-1}$ with width at half maximum of about 10 cm$^{-1}$.

The first two lines can be identified as corresponding to the longitudinal optical (LO) and transverse optical (TO) phonons of GaAs [13]. We believe that the intense line corresponds to a coupled mode of longitudinal optical phonon and a hole plasmon (coupled phonon-plasmon mode — CPLP) [14], the existence of which is supported by electrical measurements showing a high concentration of free holes (see below).

Electrical measurements at 300 K showed that the Hall effect is normal (the Hall resistance linearly depends on the magnetic field strength) for laser-annealed GaMnAs layers, and the conductivity type is hole for all doses used. The electrical parameters of the layers calculated from these measurements (layer, or surface resistance, layer concentration of holes $p_s$ and their effective mobility) are presented in the Table.

The coefficient of electrical activity of Mn (the ratio $p_s$ to the ion dose $D$) decreases with $D$ increasing from 21% for $1 \cdot 10^{16}$ cm$^{-2}$ to 7% for dose $5 \cdot 10^{16}$ cm$^{-2}$. The

Electrical parameters of ion-implanted and laser-annealed GaMnAs layers at 300 K

| Ion dose, cm$^{-2}$ | $1 \cdot 10^{16}$ | $3 \cdot 10^{16}$ | $5 \cdot 10^{16}$ |
|---|---|---|---|
| Layer resistance $R_S$, $\Omega$/sq | 822 | 457 | 345 |
| Effective mobility $\mu_{\text{eff}}$, cm$^2$/V · s | 3.6 | 4.4 | 5.1 |
| Layer concentration of holes $p_s$, cm$^{-2}$ | $2.13 \cdot 10^{15}$ | $3.11 \cdot 10^{15}$ | $3.54 \cdot 10^{15}$ |

average acceptor concentrations (for a layer of 150 nm thick) are $1.4 \cdot 10^{20}$ and $2.3 \cdot 10^{20}$ cm$^{-3}$ for the indicated ion doses, respectively. The effective mobility of holes is low $\sim 3{-}5$ cm$^2$/V · s.

As the measurement temperature decreases, the resistance of the samples increases, showing generally semiconductor behavior (Figure 4). At the same time, the dependences for implantation doses $3 \cdot 10^{16}$ and $5 \cdot 10^{16}$ cm$^{-2}$reveal a clear maximum of layer resistance at certain temperature (35 and 120 K, respectively), which is usually interpreted as the Curie temperature. For Mn dose equal to $1 \cdot 10^{16}$ cm$^{-2}$, only a small kink is observed in the region 30–40 K. As the measurement temperature decreases, the Hall effect of annealed samples becomes anomalous. Figure 5 shows the magnetic field dependences of the Hall resistance $R_{\text{H}}$ (i.e., the ratio of the Hall voltage to the current) for a sample irradiated with Mn ions with dose $5 \cdot 10^{16}$ cm$^{-2}$ and annealed by laser pulse.

It can be seen that the magnetic field dependence of the Hall resistance corresponds to the known in [15] expression

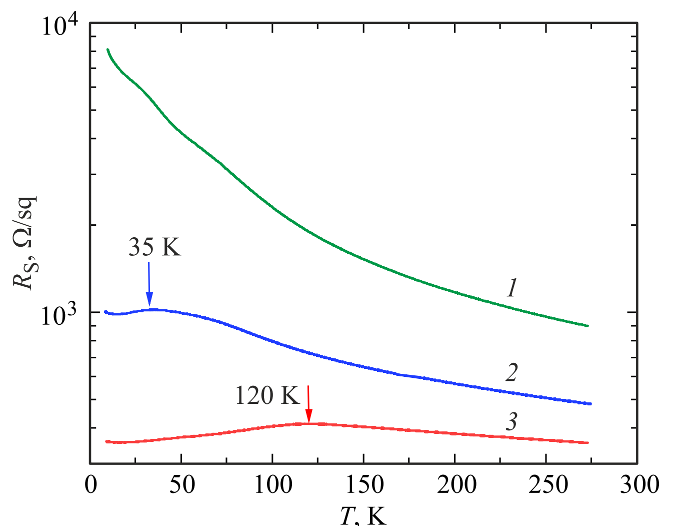


**Figure 4.** Resistance vs/measurement temperature for GaMnAs layers obtained by implantation of Mn ions with doses $1 \cdot 10^{16}$ (curve *1*), $3 \cdot 10^{16}$ (curve *2*) and $5 \cdot 10^{16}$ cm$^{-2}$ (curve *3*) followed by laser annealing.

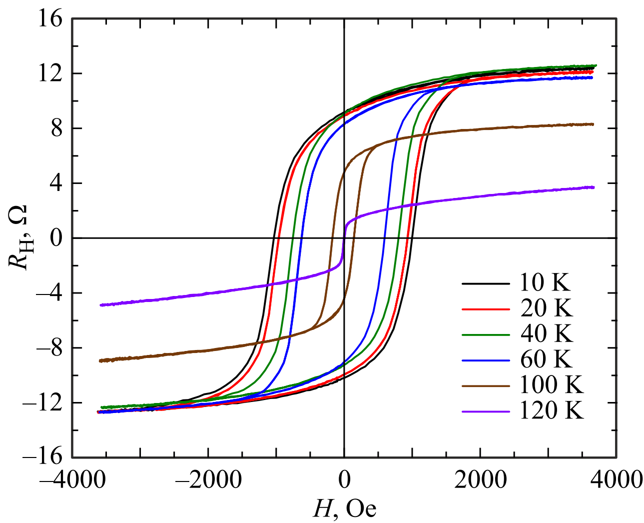


**Figure 5.** Magnetic field dependences of the Hall resistance when varying the measurement temperature for GaAs sample irradiated with Mn ions with dose $5 \cdot 10^{16}\,\mathrm{cm}^{-2}$ and annealed by laser pulse. The magnetic field was applied perpendicular to the sample plane.

for ferromagnetic materials

$$R_\mathrm{H} = (R_0/d)H + (R_a/d)M, \qquad (1)$$

where $R_0$ — normal Hall effect coefficient, $d$ — thickness of the doped layer, $R_a$ — anomalous Hall effect coefficient, $M$ — magnetization depending on the strength of the external magnetic field.

At relatively low values of the magnetic field strength, the term associated with the magnetic field dependence of magnetization predominates and has the form of a hysteresis loop. Saturation of magnetization occurs for low temperatures (10−60 K) at magnetic fields about 2000 Oe, and then with $H$ increasing the magnetic field dependence $R_\mathrm{H}$ is determined by the first, linear in the field, term of equation (1). The hysteresis loop is observed at measurement temperatures up to 100 K, and the nonlinearity of the Hall resistance is observed even at 120 K. As the temperature decreases from 100 to 10 K, the coercive field monotonically increases, and the saturation attainment field also increases. From the slope of the magnetic field dependence $R_\mathrm{H}$ in the region of magnetization saturation, one can estimate the layer concentration of holes at low temperatures. For the curve shown in Figure 5 for 100 K this estimate gives the value $p_s = 2.3 \cdot 10^{14}\,\mathrm{cm}^{-2}$, which is by an order of magnitude lower than for 300 K. Assuming that the layer resistance at 100 K is about 400 Ω/sq, the approximate estimate of hole mobility gives the value $\sim 70\,\mathrm{cm}^2/\mathrm{V} \cdot \mathrm{s}$ for this temperature.

Samples obtained by irradiation with Mn ions with doses $1 \cdot 10^{16}$ and $3 \cdot 10^{16}\,\mathrm{cm}^{-2}$ followed by laser annealing show an anomalous Hall effect with a hysteresis loop up to 40 K.

As can be seen from Figure 5, at temperatures below the Curie temperature the anomalous Hall effect generally predominates, and the Hall resistance in this case can be approximately considered as $R_\mathrm{H} \approx R_a M/d$. This approximation is used to determine spontaneous Hall resistance $R_\mathrm{H}^\mathrm{S}$ which is proportional to spontaneous magnetization $M_\mathrm{S}$ and characterizes ferromagnetic ordering. Arrott's procedure [16] was applied comprising plotting dependence $M^2(H/M)$ and finding $M_\mathrm{S}$ by extrapolation of its linear portion up to the intersection with the axis of ordinates. $R_\mathrm{H}^\mathrm{S}$ was calculated in the same way, but using dependences $R_\mathrm{H}^2(H/R_\mathrm{H})$. If linear extrapolation $R_\mathrm{H}^2(H/R_\mathrm{H})$ to value $H = 0$ gives $(R_\mathrm{H}^\mathrm{S})^2 > 0$, then ferromagnetic ordering is present for this measurement temperature. If value $(R_\mathrm{H}^\mathrm{S})^2 < 0$, then the ferromagnetism is absent.

Figure 6 shows the dependences $R_\mathrm{H}^\mathrm{S}(T)$ obtained by the method described above, they make it possible to determine the temperature of the ferromagnetic/paramagnetic phase transition for each sample studied. Comparison of the data obtained with the results of the Curie temperature estimation by he position of the maximum on the corresponding temperature dependences of the resistance (Figure 4) shows that the coincidence in the determination of $T_\mathrm{C}$ by both methods is observed only for the sample with the Mn implantation dose $D = 5 \cdot 10^{16}\,\mathrm{cm}^{-2}$, and for the sample with lower implantation dose ($3 \cdot 10^{16}\,\mathrm{cm}^{-2}$), the estimate $T_\mathrm{C}$ by the position of the maximum resistance gives the underestimated value (35 versus 60 K).

Figure 7 shows the magnetic field dependences of magnetoresistance (MR) for the sample obtained at the maximum dose of Mn ions implantation.

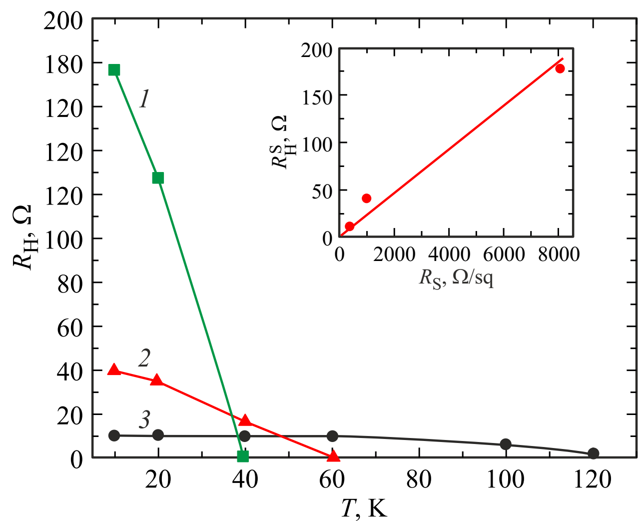


**Figure 6.** Spontaneous Hall resistance vs. measurement temperature, calculated using the Arrott's procedure, for GaAs samples obtained by implantation of Mn ions followed by laser annealing, for three irradiation doses. Curve *1* corresponds to the dose $1 \cdot 10^{16}\,\mathrm{cm}^{-2}$, curve *2* — $3 \cdot 10^{16}\,\mathrm{cm}^{-2}$ and curve *3* — dose $5 \cdot 10^{16}\,\mathrm{cm}^{-2}$. The insert shows the relationship between the value of the spontaneous Hall coefficient and the surface resistance of layers at measurement temperature of 10 K (the dots show experimental results, and the straight line is the linear approximation).

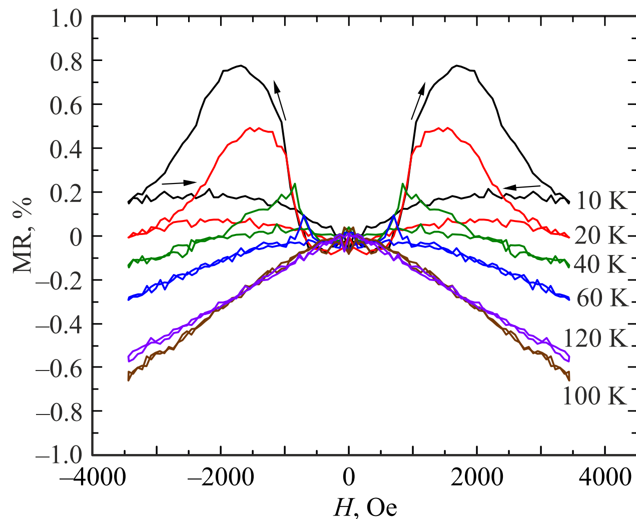


**Figure 7.** Magnetic field dependences of the magnetoresistance *H* of GaAs layers irradiated with Mn ions with dose $5 \cdot 10^{16}\,\text{cm}^{-2}$ and annealed by laser pulse during varying the measurement temperature. The magnetic field was applied perpendicular to the sample plane.

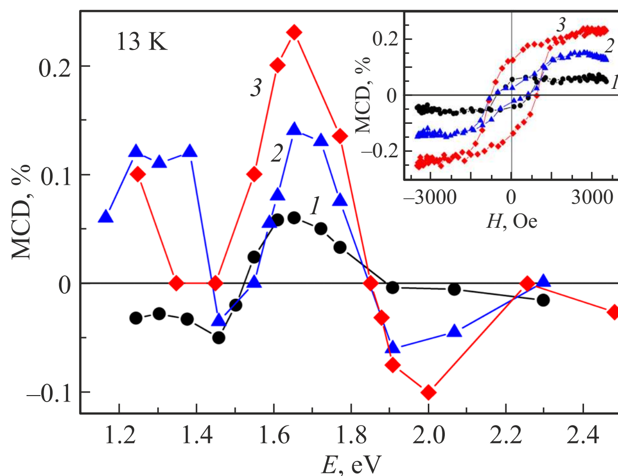


**Figure 8.** Spectral dependences of the MCD of annealed GaMnAs samples obtained by ion implantation with different doses: $1 \cdot 10^{16}$ (curve *1*), $3 \cdot 10^{16}$ (curve *2*) and $5 \cdot 10^{16}\,\text{cm}^{-2}$ (curve *3*). The insert shows the MCD signal at 1.66 eV vs. the magnetic field for the above-mentioned implantation doses. Measurement temperature = 13 K; the magnetic field is applied perpendicular to the surface of the samples.

It can be seen that, in general, the magnetoresistance is negative up to the Curie temperature, and at the lowest temperatures near zero magnetic field there is a positive section of MR („ears“ appear). Arrows indicate direction of magnetic field change (bypass). At measurement temperatures up to 60 K, the hysteretic behavior of the magnetoresistance is noticeable. The position of the local maximum of MR on the magnetic field scale approximately coincides with the saturation field (~ 1700 Oe at 10 K). The value of positive MR in this local maximum reaches 0.8% at 10 K. With temperature increasing the local maxima shift to zero magnetic field and decrease through height (700 Oe and 0.08% at 60 K). A similar type of magnetic field dependence of MR (the presence of a positive component at low magnetic fields and a negative component) is characteristic of the manifestation of anisotropic magnetoresistance in ferromagnetic systems [17,18].

At temperatures of 100 and 120 K magnetoresistance becomes negative. This behavior of the dependences MR($H$), as well as the appearance of the hysteresis loop in the magnetic field dependences of the Hall effect, is evidence of the ferromagnetic properties of GaMnAs layers obtained using the described technology.

A generally accepted method of proving one or another nature of ferromagnetism in layers of semiconductors doped with transition metal impurities is the study of magnetic circular dichroism (MCD) [19]. Figure 8 shows the MCD spectra at 13 K in magnetic field of 3500 Oe at different photon energies for GaMnAs layers obtained by implantation with different doses of Mn ions and annealed by a laser pulse. A pronounced spectral dependence of the MCD is observed: a positive peak at a quantum energy of approximately 1.66 eV and a negative peak at ~ 2 eV, which is especially noticeable for the maximum implantation dose. The intensities of these peaks increase with dose increasing of irradiation with Mn ions. The insert to Figure 8 shows the magnetic field dependences of the magnitude of the MCD signal obtained at photon energy of 1.66 eV. Magnetic field dependences are hysteresis; in this case, the MCD signal in saturation also increases with the ion dose. The Curie temperature of structures determined from MCD studies by varying the measurement temperature is in good agreement with the Curie temperature obtained from magnetic transport studies. For samples implanted and annealed by laser pulse the magnetization was also studied at 300 K using the method of alternating magnetic field gradient, which showed the absence of ferromagnetic signal (only a linear magnetic field dependence of magnetization was observed).

## 4. Discussion of results

First, let's pay attention to the fact that the experimental depth distribution of implanted Mn (Figure 1, profile *2*) before laser annealing has a bell-like shape, which does not differ too much from the distribution calculated using the SRIM code and modified taking into account ion sputtering (Figure 1, profile *1*). As it was expected, at implantation energy of manganese ions of 180 keV, the position of the maximum of the experimental depth distribution (~ 80 nm) is somewhat less than the value $R_p = 105.2\,\text{nm}$, calculated using the SRIM program not considering the ion etching. Of course, the experimental profile shall not shift toward the surface by the amount of the ion-etched down layer ($d_s = 48\,\text{nm}$ for the ion dose $3 \cdot 10^{16}\,\text{cm}^{-2}$), since we are dealing with a dynamic process

when, as the dose of ions increases, both the GaAs layer, already containing manganese atoms, is etched down, and the ions travel to an average depth $R_p$, measured from the new surface. We only state that the resulting ion doses, taking into account etching losses, are, according to our calculations, $9.83 \cdot 10^{15}$ (the dose set by the operator $D = 1 \cdot 10^{16}\,\text{cm}^{-2}$), $2.83 \cdot 10^{16}$ ($D = 3 \cdot 10^{16}\,\text{cm}^{-2}$) and $4.38 \cdot 10^{16}\,\text{cm}^{-2}$ ($D = 5 \cdot 10^{16}\,\text{cm}^{-2}$).

The result of irradiation with Mn ions at the used doses is amorphization of the implanted GaAs layer. This is confirmed by the shape of RS spectrum shown in Figure 3 (curve *1*). Similar RS spectra were obtained earlier by other authors during ion irradiation of GaAs: a broad line centered at $255\,\text{cm}^{-1}$ for implantation of ions $Si^+$ with energy of 100 keV and dose $3 \cdot 10^{15}\,\text{cm}^{-2}$ (above the amorphization dose) [20] and also wide band at $\sim 260\,\text{cm}^{-1}$ for implantation of ions $As^+$ with energy of 270 keV and dose of $3.2 \cdot 10^{14}\,\text{cm}^{-2}$(above the amorphization threshold) [21].

Laser annealing, performed to restore the crystalline structure of the layer and electrical activation of Mn atoms, leads to change in the RS spectrum (Figure 3, curve *2*): RS signal intensity increases, and the dominant line significantly narrows. If we used the electrically inactive type of ions (in [22] these are isovalent ions In with dose higher than the amorphization dose), then after laser annealing two narrow peaks should be observed in RS spectrum, corresponding to LO- and TO-modes (as in [22]). But in our case, due to the high concentration of electrically active Mn, which acts as the acceptor and ensures hole concentration higher than $10^{20}\,\text{cm}^{-3}$, these LO and TO modes practically do not appear, and the coupled phonon-plasmonic mode predominates in the spectrum similarly to paper [14]. Thus, we can state that the selected conditions of annealing with excimer laser pulse (energy density $300\,\text{mJ/cm}^2$) ensure restoration of the GaAs crystal structure after ion implantation. This conclusion is also confirmed by electrical measurements, since the experimental Hall mobility of holes at 300 K is $\sim 5\,\text{cm}^2/\text{V} \cdot \text{s}$ (see Table), and this value noticeably exceeds the mobility during the hopping mechanism of carrier transfer ($< 1\,\text{cm}^2/\text{V} \cdot \text{s}$). Calculation of the holes mobility in GaAs with the predominance of scattering on ionized carriers using formula (116) from [23] gives for the acceptor concentration $2.3 \cdot 10^{20}\,\text{cm}^{-3}$ the mobility value $1.1\,\text{cm}^2/\text{V} \cdot \text{s}$, which even is below the results of our measurements.

As a result of laser annealing, dramatic changes in the profile occurred: a significant part of the implanted Mn atoms was displaced to the surface.

When exposed to laser pulse with a wavelength of 248 nm, even in single-crystal GaAs, the depth of light absorption is approximately 5 nm [24]. In GaAs amorphized by ion implantation, the light shall be absorbed at an even smaller distance from the surface [25]. The energy released during the absorption of light is converted into heat, spreading from the surface into the depth of the sample. It was shown [9] that at an excimer laser pulse energy of $260\,\text{mJ/cm}^2$ GaAs melts to a depth of 150 nm. Meanwhile, it was established [25] that the melting temperature of amorphized GaAs (*a*-GaAs) is approximately by 160 K lower than that of crystalline GaAs, so we can assume that in our case the melting depth irradiated with GaAs ions is approximately equal to or greater the implantation depth.

After the end of the laser pulse the sample begins to cool, and the crystallization front moves from the undisturbed single-crystal substrate to the surface. According to estimates [12,25], the crystallization front moves with speed of up to 10 m/s. At such a high speed of the crystallization front movement, the distribution coefficient defined as the ratio of the impurity concentration in the solid phase to the concentration in the melt ($K = C_S/C_L$) at the liquid/solid interface, and which in the equilibrium case (Mn in GaAs) is equal to 0.05 [3], can increase significantly. However, Mn segregation during PLA to the surface (Figure 1, curve *3*) clearly indicates that $K_{Mn} < 1$ even under nonequilibrium conditions of laser annealing.

Calculation of the temperature distribution during PLA in the case of ion implantation is difficult, since many data for amorphous GaAs are unknown, primarily the dependence of thermal constants on temperature.

Segregation-type profiles for Mn in GaAs after PLA were already noted in the literature [12,17]. Note, however, that according to [17] Mn atoms in this near-surface layer are in electrically and magnetically inactive state (possibly in the form of an oxide) and do not affect electrical and galvanomagnetic measurements.

We can state that GaMnAs layer formed under the selected conditions of implantation and pulsed laser annealing is a ferromagnetic semiconductor with Curie temperature that depends on the ion dose. Evidence of the ferromagnetic state is: hysteresis loops on the magnetic field dependences of the Hall effect and the magnitude of the magnetic circular dichroism signal, negative magnetoresistance, and the presence of spontaneous Hall coefficient calculated using the generally accepted Arrott's procedure.

The insert to Figure 6 shows the relationship between the surface resistance of GaMnAs layers obtained at three doses of Mn ion implantation and the corresponding values of the spontaneous Hall coefficient. A direct proportionality between the indicated quantities is visible, which indicates the predominance of the skew scattering mechanism in the occurrence of the anomalous component of the Hall effect [1].

The pronounced spectral dependence of magnetic circular dichroism for samples with GaMnAs layers obtained by us (Figure 8) is characteristic of single-phase GaMnAs layers [26]. The absence at room temperature of measurements of the ferromagnetic magnetization signal also indicates the absence in the formed layers of ferromagnetic clusters such as MnAs or MnGa, for which the Curie temperature is higher than room temperature [5].

A separate discussion is required for the difference in determining the Curie temperature by different methods: by the peak of the temperature dependence of the resistance, by the temperature dependence of the spontaneous Hall coefficient, and by the presence of hysteresis loop in the

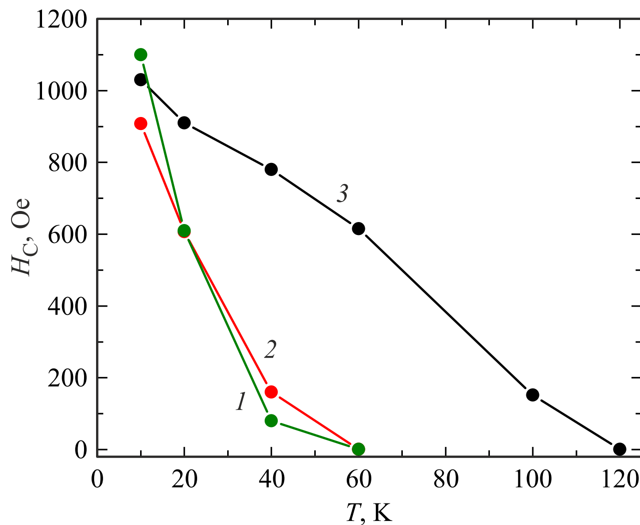


**Figure 9.** Coercive field in the magnetic field dependences of the anomalous Hall effect for three doses of Mn ions implantation: $1 \cdot 10^{16}$ (*1*), $3 \cdot 10^{16}$ (*2*) and $5 \cdot 10^{16}\,\text{cm}^{-2}$ (*3*) at different measurement temperatures.

magnetic field dependence of the Hall effect. Figure 9 shows data on the coercive field dependence on temperature for three Mn ion implantation doses used in the paper.

It can be seen that, taking into account the temperature step used in the experiment when measuring the Hall effect, the data shown in Figure 9 are in good agreement with the results of calculations of the spontaneous Hall coefficient (Figure 6): $\sim 40\,\text{K}$ for dose $1 \cdot 10^{16}\,\text{cm}^{-2}$, $60\,\text{K}$ for dose $3 \cdot 10^{16}\,\text{cm}^{-2}$ and $120\,\text{K}$ for dose $5 \cdot 10^{16}\,\text{cm}^{-2}$.

Note, however, for the results of measurements of the temperature dependence of the surface resistance that although with implantation dose increasing the peak shifts to higher temperatures, there is no strict correlation with the Curie temperature determined from measurements of the Hall effect at low temperatures. This behavior contradicts the measurement data of the dependences $R(T)$ for GaMnAs samples grown by LT-MBE method when the Mn concentration varied from 2 to 6% [27]. In that paper a good correlation was observed between the position of the peak $R(T)$ and measurements of the temperature dependence of magnetization and temperature diffusivity, which indicated that the critical point determined by the $R(T)$method corresponded to the temperature of the phase transition of second kind, i.e. Curie temperature. The reason for the difference in the position of the peak $R(T)$ for the dose $3 \cdot 10^{16}\,\text{cm}^{-2}$ from the Curie temperature ($\sim 60\,\text{K}$), determined by us by other methods, and the peak absence for the dose $1 \cdot 10^{16}\,\text{cm}^{-2}$ is not yet clear and requires additional studies.

## 5. Conclusion

Thus, GaMnAs layers formed by implantation into semi-insulating GaAs of ions $\text{Mn}^+$ with energy of $180\,\text{keV}$, doses from $1 \cdot 10^{16}$ to $5 \cdot 10^{16}\,\text{cm}^{-2}$ and subjected to single annealing pulse of the excimer KrF laser, reveal both semiconductor and ferromagnetic properties. The *p*-type conductivity, high hole concentration (up to $\sim 2.3 \cdot 10^{20}\,\text{cm}^{-3}$ depending on the dose), temperature dependence of the layer resistance of the semiconductor type, Hall mobility of charge carriers $\sim 5\,\text{cm}^2/\text{V} \cdot \text{s}$, approximately corresponding to the measured acceptor concentration, the Raman scattering spectrum with coupled phonon-plasmon mode characterizes GaMnAs as the semiconductor. The ferromagnetic behavior of GaMnAs is proven by measurements of the anomalous Hall effect with hysteresis-type magnetic field dependences, observations of negative magnetoresistance with anisotropy at low magnetic fields, the characteristic spectral dependence of magnetic circular dichroism, and spontaneous Hall resistance. In this case, the Curie temperature of GaMnAs as a ferromagnet increases monotonically with the ion dose and reaches $120\,\text{K}$ at $D = 5 \cdot 10^{16}\,\text{cm}^{-2}$. X-ray diffraction studies confirm the improvement in the crystal structure of the layers as a result of laser annealing, and profiling of the impurity through the depth of the doped layer using secondary ion mass spectrometry shows significant segregation of Mn atoms to the surface in this process.

### Funding

This study was supported financially by the Russian Science Foundation (project No. 23-29-00312). SIMS studies were carried out on the equipment of the Center for Collective Use „Diagnostics of Micro- and Nanostructures“. X-ray diffraction studies were carried out using the equipment of the Center for Collective Use „Physics and Technology of Micro- and Nanostructures“ in the laboratory for diagnostics of radiation defects in solid-state nanostructures of the Institute for Physics of Microstructures of the Russian Academy of Sciences.

### Conflict of interest

The authors declare that they have no conflict of interest.

## References

[1] T. Dietl, H. Ohno. Rev. Mod. Phys. **86**, 187 (2014).
[2] T. Jungwirth, T. Wunderlich, V. Novac, K. Olejnik, B.L. Gallagher, R.P. Campion, K.W. Edmonds, A.W. Rushforth, A.J. Ferguson, P. Nemec. Rev. Mod. Phys. **86**, 855 (2014).
[3] V.I. Fistul, Atomy legiruyushchikh primesey v poluprovodnikakh, Fizmatlit, M. (2004), 432 s. (in Russian).
[4] J. Shi, J.M. Kikkawa, D.D. Awschalom, G. Medeiros-Ribeiro, P.M. Petroff, K. Babcock. J. Appl, Phys. **79**, 5296 (1996).
[5] O.D.D. Couto, Jr., M.J.S.P. Brasil, F. Iikawa, C. Giles, C. Adriano, J.R.R. Bortoleto, M.A.A. Pudenzi, H.R. Gutierrez, I. Danilov. Appl. Phys. Lett. **86**, 071906 (2005).
[6] Yu.A. Danilov, A.V. Kruglov, M. Behar, M.C. dos Santos, L.G. Pereira, J.E. Schmidt. FTT **47**, *9*, 1567 (2005).

[7] S.S. Khludkov, O.B. Koretskaya. Izv. vuzov, Fizika **28**, 107 (1985). (in Russian).
[8] M.A. Scarpulla, O.D. Dubon, K.M. Yu, O. Monteiro, M.R. Pillai, M.J. Aziz, M.C. Ridgway. Appl. Phys. Lett. **82**, 1251 (2003).
[9] D. Bürger, S. Zhou, M. Pandey, C.S. Viswanadham, J. Grenzer, O. Roshchupkina, W. Anwand, H. Reuther, V. Gottschalch, M. Helm, H. Schmidt. Phys. Rev. B **81**, 115202 (2010).
[10] Yu.A. Danilov, H. Boudinov, O.V. Vikhrova, A.V. Zdoroveishchev, A.V. Kudrin, S.A. Pavlov, A.E. Parafin, E.A. Pitirimova, R.R. Yakubov. FTT **58**, 2140 (2016). (in Russian).
[11] J.F. Ziegler, J.P. Biersack, U. Littmark. The Stopping and Range of Ions in Solids. Pergamon Press, N.Y. (1985).
[12] S. Zhou. J. Phys. D **48**, 263001 (2015).
[13] I.T. Yoon, T.W. Kang. J. Magn. Magn. Mater. **321**, 2257 (2009).
[14] W. Limmer, M. Glunk, S. Mascheck, A. Koeder, D. Klarer, W. Schoch, K. Thonke, R. Sauer, A. Waag. Phys. Rev. B. **66**, 205209 (2002).
[15] N. Nagaosa, J. Sinova, S. Onoda, A.H. MacDonald, N.P. Ong. Rev. Mod. Phys. **82**, 1539 (2010).
[16] A. Arrott. Phys. Rev. **108**, 1394 (1957).
[17] M.A. Scarpulla, R. Farshchi, P.R. Stone, R.V. Chopdekar, K.M. Yu, Y. Suzuki, O.D. Dubon. J. Appl. Phys. **103**, 073913 (2008).
[18] A.V. Kudrin, O.V. Vikhrova, Yu.A. Danilov. PZhTF **36**, *11*, 46 (2010). (in Russian).
[19] K.J. Yee, R. Chakarvorty, W.L. Lim, X. Liu, M. Kutrowski, L.V. Titova, T. Wojtowicz, J.K. Furdyna, M. Dobrowolska. J. Supercond. Nov. Magn. **18**, 131 (2005).
[20] U.V. Desnica, I.D. Desnica-Franković, M. Ivanda, K.Furić, T.E. Haynes. Phys. Rev. B **55**, 16205 (1997).
[21] K.K. Tiong, P.M. Amirtharaj, P.H. Pollak, D.E. Aspnes. Appl. Phys. Lett. **44**, 122 (1984).
[22] J. Sapriel, Y. Nissim, B. Joukoff, J. Oudar, S. Abraham, R. Beserman. J. Phys. Coll. **45**, C5-75 (1984).
[23] J.S. Blakemore. J. Appl. Phys. **53**, R123 (1982).
[24] I.L. Kalentyeva, O.V. Vikhrova, Yu.A. Danilov, M.V. Dorokhin, B.N. Zvonkov, Yu.M. Kuznetsov, A.V. Kudrin, D.V. Khomitsky, A.E. Parafin, P.A. Yunin, D.V. Danilov. J. Magn. Magn. Mater. **556**, 169360 (2022).
[25] T. Kim, M.R. Pillai, M.J. Aziz, M.A. Scarpulla, O.D. Dubon, K.M. Yu, J.W. Beeman, M.C. Ridgway. J. Appl. Phys. **108**, 013508 (2010).
[26] K. Ando, H. Saito, K.C. Agarwal, M.C. Debnath, V. Zayets, Phys. Rev. Lett. **100**, 067204 (2008).
[27] Sh.U. Yuldashev, Kh.T. Igamberdiev, Y.H. Kwon, S. Lee, X. Liu, J.K. Furdyna, A.G. Shashkov, T.W. Kang. Phys. Rev. B. **85**, 125202 (2012).

*Translated by 123*